Influence of nanochannel structure on helium-vacancy cluster evolution and helium retention

Qin, Wenjing
Jin, Shuoxue
Cao, Xingzhong
Wang, Yongqiang
Peres, Paula
Choi, Seo-Youn
Jiang, Changzhong
Ren, Feng

To be published in: Journal of Nuclear Materials

DOI to publisher's version: 10.1016/j.jnucmat.2019.151822

Permalink to record: http://permalink.lanl.gov/object/view?what=info:lanl-repo/lareport/LA-UR-19-30363

Journal Pre-proof

Influence of nanochannel structure on helium-vacancy cluster evolution and helium retention

Wenjing Qin, Shuoxue Jin, Xingzhong Cao, Yongqiang Wang, Paula Peres, Seo-Youn Choi, Changzhong Jiang, Feng Ren

PII: S0022-3115(19)30336-8

DOI: https://doi.org/10.1016/j.jnucmat.2019.151822

Reference: NUMA 151822

To appear in: *Journal of Nuclear Materials*

Received Date: 10 March 2019

Revised Date: 18 September 2019

Accepted Date: 28 September 2019

Please cite this article as: W. Qin, S. Jin, X. Cao, Y. Wang, P. Peres, S.-Y. Choi, C. Jiang, F. Ren, Influence of nanochannel structure on helium-vacancy cluster evolution and helium retention, *Journal of Nuclear Materials* (2019), doi: https://doi.org/10.1016/j.jnucmat.2019.151822.

Influence of nanochannel structure on helium-vacancy cluster evolution and helium retention

Wenjing Qin[1,2], Shuoxue Jin[3], Xingzhong Cao[3], Yongqiang Wang[4,*], Paula Peres[5], Seo-Youn Choi[5], Changzhong Jiang[1], Feng Ren[1,*]

[1] School of Physics and Technology, Center for Ion Beam Application and Center for Electron Microscopy, and Hubei Nuclear Solid Physics Key Laboratory, Wuhan University, Wuhan 430072, China.

[2] Synergetic Innovation Center for Quantum Effects and Application, Key Laboratory of Low Dimensional Quantum Structures and Quantum Control, School of Physics and Electronics, Hunan Normal University, Changsha 410081, China.

[3] Institute of High Energy Physics, Chinese Academy of Sciences, Beijing 100049, China.

[4] Materials Science and Technology Division, Los Alamos National Laboratory, Los Alamos, New Mexico 87545, USA.

[5] CAMECA, 29 quai des Grésillons, Gennevilliers 92230, France.

* E-mail: fren@whu.edu.cn; yqwang@lanl.gov

Abstract

In the fusion reactors, plasma facing materials (PFMs) will be bombarded by large amounts of energetic particles, including helium (He) atoms. These metal-insoluble He atoms are prone to self-trapping or are trapped by vacancies, dislocation cores or grain boundaries, aggregating to form high concentration He bubbles which leads to serious degradation of the PFMs' properties. Studying the initial stages of He-defect interactions becomes increasingly important because it not only helps us understand

the formation mechanism of He bubbles but also provides insight to help design new irradiation-resistant PFMs. In this work, we used the positron annihilation Doppler broadening spectroscopy (DBS) and secondary ion mass spectrometry (SIMS) to explore the evolutions of the interactions between vacancy-type defects and He and the retention of He in the nanochannel W film irradiated with 190 keV He^+ ions to different fluences under different temperatures. It is found that the presence of a nanochannel structure accelerates the release of He from the film even at low irradiation fluences, and the release of He is significantly enhanced at higher fluences, thus inhibiting or delaying the formation of large He-vacancy clusters in the nanochannel W film. Both irradiation fluence and temperature have significant influence on the formation and evolution of He-vacancy clusters, and the evolution of these microstructure also causes hardness changes.

Keywords: tungsten; nanochannel; vacancy-type defects; He-retention; hardness

1. Introduction

Tungsten (W) is considered as one of the most promising plasma facing materials (PFMs), and ITER has planned to use an all-W divertor in the final design. However, in the extreme fusion environment, the large numbers of helium (He) atoms that are produced by deuterium (D) and tritium (T) reaction or transmuted by 14.1 MeV neutrons through (n, alpha) reactions will seriously impact the PFMs. In addition, neutron irradiation also produces displacement damages including vacancies and other extended defects. Accumulation of He atoms will lead to the formation of He bubbles and even surface blisters in W, which results in the embrittlement and hardening of W and eventually reduces the service life of W as a PFM [1]. Some theoretical calculations have indicated that because the He atom has a closed-shell

electronic structure and is insoluble in W, it has a strong tendency to bind with other He atoms as well as pre-existing defects such as vacancies or dislocations to form clusters. The small clusters continue to grow by trapping He atoms or mobile He clusters until the internal pressure is high enough to kick out a W self-interstitial atom and create a vacancy. The formed He-vacancy clusters act as a nucleus for the growth of He bubbles by continuing to absorb mobile He atoms or clusters [2-4]. Moreover, the relative rates of nucleation and growth of He bubbles are affected by ion flux, temperature, vacancy concentration, and even the orientation of W surfaces [5-7]. Therefore, the nucleation and growth of He bubbles in W is a very complex process, and it is also a concern in fusion research.

In our previous works [8-10], we proposed a new strategy to increase the irradiation resistance of W by introducing nanochannel structure aiming to solve the problem of the He bubbles accumulation. Through a series of comparative experiments with ordinary polycrystalline W, it was found that the density and size of He bubbles in the nanochannel W films are relatively small irradiated by low-flux He^+ ions to high fluence at room or high temperature, which is due to partial He release from the films (measured by elastic recoil detection). We believe that a nanochannel structure existed in W film can effectively release He and inhibit the rapid growth of He bubbles. It is well known that the nucleation of He bubbles is as a critical surface existed in the atomic scale (He-vacancy clusters) and mesoscopic scale (He bubbles) [3]. However, at present, there is no relevant experimental study on the mechanism of the influence of nanochannel structures on the He bubbles nucleation at initial stage of He-irradiation. Thus, it is very important to investigate the initial stages of He bubbles formation in the nanochannel W film, which could help us to understand the underlying physics of how a nanochannel structure inhibits the growth of He bubbles.

At present, it is very difficult to study the evolutions of vacancies, He_nV_m clusters or other vacancy-type defects by using conventional characterization means such as transmission electron microscope (TEM) due to their very small sizes. Positron annihilation Doppler broadening spectroscopy (DBS) is a powerful and sensitive method to probe vacancy-type defects [11]. Moreover, it is also a very suitable tool to detect the depth dependence of vacancy-type defects and microstructures in solid targets with a variable energy positron beam [12]. Depth profiling measurements using dynamic secondary ion mass spectrometry (SIMS) were also performed in this study. Offering high sensitivity and high depth resolution, dynamic SIMS has proven extremely useful for studying diffusion and migration mechanisms of trace elements in nuclear materials [13].

In this work, we take advantages of DBS and SIMS to explore the evolution of He-vacancy complexes and He retention in nanochannel W films at low fluences under different irradiation environments. Information about vacancy-type defects along with relevant mechanical hardness data are used to gain a better understanding of the early stages of He bubble formation and evolution.

2. Experimental

2.1. Materials Preparation and Irradiation

Nanochannel W film (about 850 nm thick) was deposited on the silicon (100) wafer at 600 ºC with a source power of 150 W by using ultrahigh vacuum DC magnetron sputtering deposition (ULVAC, ACS-4000-C4), where, its density of 17.46 g/cm^3 was measured by the Rutherford backscattering spectrometry (RBS), lower than that of conventional pure ordinary polycrystalline W (19.35 g/cm^3). TEM image of the nanochannel W film is shown in Fig. 1a. Clearly, the W film is composed of many

columnar crystals with nanochannels existing between the columnar crystals. Surface roughness of the deposited film measured by atomic force microscopy (AFM) is about 8 nm.

The He^+ ion irradiation experiments were performed on a 200 kV ion implanter (LC22-100-01, Beijing Zhongkexin Electronics Equipment Co., Ltd) at the Center for Ion Beam Application, Wuhan University. In order to avoid the effect of positron and surface interactions on the real distribution of vacancy-type defects in the damage region, and to better compare with the results previously reported in Refs. [14, 15], the incident energy of He^+ ion beam was set at 190 keV. The nanochannel W films were irradiated at room temperature (RT, about 25 °C) with an ion flux of about 1.5×10^{13} ions/cm^{2}s to relatively low fluences of 5×10^{15}, 1×10^{16} and 5×10^{16} ions/cm^2, respectively. In addition, the films were also irradiated at 300 or 600 ºC to the same fluence of 5×10^{16} ions/cm^2 to study the influence of temperature on the evolution of defects. Depth profiles of He atom, vacancy and He/V ratio in the irradiated nanochannel W film are shown in Fig. 1b, as calculated by SRIM-2013 using the "Quick Kinchin-Pease" mode and the displacement threshold energy of the W atom at 90 eV [16]. It should be noted that the actual number of vacancy clusters can be significantly less since large amount of vacancies are annihilated by interstitial atoms during the cascade quenching. Clearly, the He/V ratio increases with increasing depth, indicating that the incident He atoms may be more easily trapped by vacancies near the surface while are more inclined to self-trapping at the end of ion range [17]. Maximum displacement per atom (dpa) is 0.1 at the depth of around 350 nm and the peak He concentration is 0.61 at.% at the depth of around 434 nm when the fluence is 1×10^{16} ions/cm^2.

2.2. Doppler broadening spectrometry (DBS)

To investigate the evolutions of vacancy-type defects in the nanochannel W film, DBS measurements were carried out at RT with an energy-variable slow positron beam facility at the Institute of High Energy Physics, Chinese Academy of Sciences. The slow positron beam facility uses the ^{22}Na radioactive source and the emitted positrons are first moderated by a single crystal W and then post accelerated to different energies. The incident positron energies used for this study was ranged from 0.18 to 20.18 keV, and the corresponding positron annihilation depth was estimated by the following empirical formula[18]:

$$\mathrm{R} = \left(\frac{40}{\rho}\right) E^{1.6} \tag{1}$$

where R is the incident depth (nm), ρ is the density of material (g/cm^3), E is the incident positron energy (keV). From Eq. (1), the mean incident depth of positron at 20.18 keV in the W film is approximately 280 nm. Note that according to the depth profile of positron implanted in W, the positrons with energies of 0.18-20.18 keV can probe the whole damaged region of 190 keV He^+ ions [19, 20].

The 511 keV gamma ray detection in DBS measurement is done through the high purity germanium detector (HPGe). The DBS often uses the *S* and *W* parameters to characterize the nature of annihilation. The *S* parameter is defined as the ratio of the central low momentum area of the spectrum (510.2-511.8 keV) to the total spectrum (499.5-522.5 keV), and mainly reflects the information of positron annihilation with valence electrons, e.g. sensitive to the density and type of open-volume defects. On the other hand, the *W* parameter is defined as the ratio of the two flanks high momentum regions (513.6-516.9 keV and 505.1-508.4 keV) to the total spectrum and represents the information of core electrons, e.g. sensitive to the chemical surrounding at the annihilation sites. If there are vacancy-type defects in the material, the absence

of atoms will lead to a decrease of the core electrons' density and a relative increase of the density of valence electrons, resulting in a narrowing of the spectrum to make the *S* parameter value larger and *W* parameter value smaller [14, 18, 21].

2.3. SIMS measurement

He depth profiles in the irradiated nanochannel W films were obtained by SIMS on the CAMECA IMS 7f-Auto using Cs^+ primary ions at 5 keV impact energy and collecting secondary positive $CsHe^+$ ions. The detection of $CsHe^+$ molecule ion is an efficient method to overcome the high first ionization potential of He [22]. The incidence angle was 45°, the primary beam current was approximately 105 nA, the raster size was 150×150 μm^2, and the analysed area was 33 μm in diameter. A mass resolving power (about 2000) was used to decrease the contribution of the $^{133}Cs^+$ peak's tail at the neighbouring $^{133}Cs^4He^+$ species, and the energy bandwidth was set to 75 eV. The depth calibration was based on a crater depth measurement performed after the SIMS analyses using a surface profilometer, and by normalizing the sputtering rate for each profile to the average primary current during the acquisition. For all profiles, a constant sputtering rate (approximately 103 nm/min) was applied over the whole sputtered depth. The same Relative Sensitivity Factor (RSF) (2.72×10^{26} atom/cm^3) was applied to perform the concentration calibration of the He profiles. Two depth profiling measurements were performed on each sample.

2.4. Nanoindentation

The hardness behaviors of pristine and irradiated samples were characterized using continuous stiffness measurement (CSM) method on an Agilent Nanoindenter G200 equipped with a diamond Berkovich tip. At least twenty indentation points were selected to get an average hardness value. The maximum indentation depth was set to 600 nm with an indentation strain rate of 0.05 s^{-1}. Testing temperature was controlled

at 20±1 °C.

3. Results

3.1. Evolution of vacancy-type defects

To investigate the initial stages of He bubble formation in the nanochannel W film, the evolutions of vacancy-type defects in the film was first analysed. Fig. 2 shows the *S*-*E* plots of the pristine nanochannel W film irradiated at different temperatures to several fluences. In addition, to clearly show the change of vacancy-type defects before and after irradiation, the relative *S* parameters, Δ*S*/*S*, are also shown in Fig. 2. The Δ*S*/*S* parameter is defined as follows [18]:

$$\Delta S/S = (S_{irradiated} - S_{pristine})/S_{pristine} \quad (2)$$

Obviously, *S* parameter of the pristine nanochannel W film decreases gradually from the surface (about 0.443) to a depth of around 30 nm and then increases gradually, approaching the surface *S* value at a depth of around 280 nm. However, all *S* parameters of the irradiated films first increase rapidly and then decrease with the increase of incident depth. For the films irradiated at RT, the *S* parameters increase with increasing fluence but not linearly. Meanwhile, at the mean depth region of 100-280 nm, the *S* value of the film irradiated to 5×10^{16} ions/cm^2 is close to that of the film irradiated to 1×10^{16} ions/cm^2. Compared with the film irradiated at RT, the *S* value of the film irradiated at 300 ºC only increases slightly. When the irradiation temperature increases to 600 ºC, the *S* value of the film increases dramatically, and its *ΔS/S* value is more than twice of those irradiated at RT and 300 ºC.

To further explore the evolutions of vacancy-type defects in the nanochannel W film, *W* parameter as a function of *S* parameter (*W*-*S*) for all these samples are plotted and shown in Fig. 3. Since each positron annihilation site is characterized by a typical

(*S*, *W*) couple, the corresponding (*S*, *W*) points can be fitted to a straight line if only one type of vacancy-type defect exists in the sample [23, 24]. In Fig. 3a, it is easily seen that two different lines are needed to fit the (*S*, *W*) points in the pristine nanochannel W film, suggesting that there are two different open-volume defects in the pristine film. Compared with the pristine film, the distributions of (*S*, *W*) points in all the irradiated films can be fitted reasonably well with one line, implying that all the irradiated films are dominated with one type of vacancy-type defects. Furthermore, the *S* values become larger and the corresponding *W* values become smaller in the irradiated films. For the film irradiated at RT, it is shown that the slopes of the fitted lines decrease with the increase of fluence, suggesting that the size of vacancy-type defects gradually increases with increasing He fluence. In Fig. 3b, the (*S*, *W*) points of the films irradiated at RT and 300 ºC are almost in the same line, suggesting the defect types of these two temperatures are similar. When the temperature increases to 600 ºC, the *S* (*W*) value becomes much larger (smaller), resulting in a smaller slope line formed by (*S*, *W*) points. This indicates that the higher density or larger size of vacancy-type defects are formed during the He irradiation at 600 ºC.

3.2. He retention in the film after irradiation

In addition to the analysis of vacancy-type defects evolution, the He retention in the irradiated films was also measured to further study the initial stages of He bubble formation in the nanochannel W films. Fig. 4 shows the SIMS results of He quantified depth profiles obtained in the nanochannel W films irradiated with 190 keV He^+ ions at different temperatures and fluences. Two depth profiling measurements were performed on each sample. An excellent repeatability is achieved on the film samples, so for the sake of clarity, only one profile of each sample is presented in this figure.

The He detection limit of SIMS is approximately 6×10^{17} atom/cm^3 (about 10 ppm), it is obtained from the measurement of a non-irradiated pristine nanochannel W film by averaging the quantified He signal from the surface to 1 μm depth. Note that using the RSF method in the SIMS can effectively detect the He signal even in the pressured bubbles [22]. As expected, all the He-irradiated films exhibit a Gaussian-type in-depth distribution, consistent with the He profile predicted from SRIM shown in Fig. 1b. It is clear that He retention in the films varies with the temperature and fluence. The relative He retention was obtained by integrating the He quantified signal from the surface to 1 μm depth for all depth profiles, see Table 1. Due to the lack of an external standard sample, the lowest fluence sample irradiated at RT (5×10^{15} atom/cm^2) was used as reference sample. The He retention is 0.78×10^{16} atom/cm^2 for the 1×10^{16} ions/cm^2 irradiated film at RT, and only 2.84×10^{16} atom/cm^2 for the film irradiated with higher fluence, 5×10^{16} ions/cm^2 at RT. When the temperature increases to 300 °C, the He retention in the film is almost the same as that in the film irradiated at RT. However, the He retention in the film decreases sharply to 1.65×10^{16} atom/cm^2 when the temperature further increases to 600 °C. These SIMS results show that the existence of nanochannel structures do effectively facilitate the He release from the film even if the nanochannel W film is irradiated to such a low fluence, and that the higher the irradiation fluence, the more He atoms are released. On the other hand, the He releasing rate appears to be constant between RT and 300 °C but is significantly higher at a temperature of 600 °C.

3.3. Irradiation hardening

Many defects introduced by He-irradiation will inhibit the dislocation migration, resulting in a hardness increment in the irradiated samples [25, 26]. Fig. 5a shows the variation of hardness with indentation depth for the nanochannel W film before and

after irradiation. With the increase of indentation depth, the hardness curve of the pristine film reaches to a plateau quickly. For the irradiated films, however, the hardness curves first reach the maximum, then decrease gradually until they level off. These three trends are known as the reverse indentation size effect (RISE), indentation size effect (ISE) and soft substrate effect (SSE), respectively. All the irradiated films exhibit evident hardening compared with the pristine one, and the average hardness increases with the increase of the irradiation fluence and temperature. Nix-Gao model based on the geometrically necessary dislocation can explain the normal ISE, the hardness (H) and indentation depth (h) are expressed as following:

$$H^2 = H_0^2(1 + h^*/h)^{0.5} \quad (3)$$

where H_0 is the hardness at infinite depth and h* is a characteristic length which depends on the shape of indenter [27]. To obtain the H_0 of the films, the H^2 versus 1/h curves are plotted in Fig. 5b. When the indentation depth is deeper than 100 nm, the data for the pristine film can fit to a straight line, while the irradiated films exhibit bi-linearity; that is, there is a shoulder in the region 135-170 nm. This is because the SSE of the pristine depth region is below the irradiated depth region as reported by Kasada et al. [28, 29]. Thus, the H_0 of the pristine film in the depth of h>100 nm and those of the irradiated films in the depth of 100<h<150 nm were calculated and shown in Fig. 5c. Compared with the pristine film, the hardness increments in the 5×10^{15} and 1×10^{16} ions/cm^2 irradiated films are only 0.32 and 0.50 GPa, respectively, compared with 2.30 GPa in the film irradiated to 5×10^{16} ions/cm^2. For the same 5×10^{16} ions/cm^2 fluence, the hardness increments of the films irradiated at 25, 300 and 600 °C are 2.30, 2.69 and 3.07 GPa, respectively.

4. Discussion

Positron annihilation spectroscopy can not only characterize the vacancy-type defects, but also detect the open-volumes of microstructures such as surfaces and interfaces in the materials [11, 12]. For the reported compact ordinary polycrystalline W, due to the existence of inherent defects, the *S* parameter of the pristine compact W decreases with the increase of depth and its (*S*, *W*) points are all in the one line [21, 30]. However, since the W films contain nanochannel structures, many free surfaces introduced by these nanochannel structures affect the momentum distribution of electrons, which also act as open-volumes to form positron capture centres [31]. Thus, the change of *S* (*W*) parameter in the nanochannel W film is different from the compact W. From the cross-sectional TEM image of the pristine W film (Fig. 1a), we can find the diameters of columnar crystals in the W film increase gradually with the increase of depth below the surface, meaning that the density of nanochannels at the bottom near the substrate is greater than that at the top near the surface, which leads to the increase of *S* value with the depth. From the analysis of the *W*-*S* plots, two different vacancy-type defects exist in the pristine W film. Combined with the deposition process and structural characteristics of the film, it is not difficult to see that, in addition to the existence of inherent defects, another type is nanochannel. Furthermore, there are two main reasons for the relatively large *S* values at the surface of film, as follows: one is that the positrons with low energy in the range of 0-5 keV have negative power function which is easily scattered back to the surface and interacts with the surface, these scattered positrons will be easily trapped by image surface well or defects, thus increasing the *S* value at the surface [32, 33]. Another reason is that the formation energies of vacancies and He clusters near the surface are lower than those in the bulk [34, 35], which indicates that the vacancy is more likely to form near the surface, leading to a large *S* value at the surface.

Except for the pre-existing defects in the pristine film, cascade collisions between energetic He^+ ions and W atoms during the He-irradiation can introduce large numbers of defects such as monovacancies and He-vacancy clusters, etc. which lead to the increase of *S* parameter. During 60 or 800 keV He^+ ions irradiated ordinary polycrystalline W described by Lhuillier et al., the monovacancies were first formed in the cascade collisions [20, 36, 37]. The He atoms are easily trapped by monovacancies to form He_nV_1 clusters. When the number of He atoms filled with a monovacancy exceeds the critical value, the "trap mutation" occurs by ejecting the self-interstitial W atom of the surrounding lattice to release intrinsic stress, forming a $He_{n+1}V_2$ cluster [38]. It can be inferred that, in our experiment, the major irradiation-induced defects are monovacancies. With the increase of fluence, the number of monovacancies induced by irradiation increases, and more He atoms are trapped by monovacancies and evolve to form He_nV_m clusters with increased incident number of He atoms. Because the *S* parameter is very sensitive to the n/m ratio of He_nV_m clusters, the increase of He_nV_m clusters size and/or density will lead to the increase of *S* parameter [39]. Moreover, the SIMS results show that the amount of He atoms released from the film increases with the increase of fluence. Thus, the *S* value does not increase linearly with the increase of irradiation fluence. The *S* value of the film irradiated to 5×10^{16} ions/cm^2 is similar with that of the film irradiated to 1×10^{16} ions/cm^2 at the100-280 nm region, which may be due to small He bubbles forming at the high fluence: positron annihilation is not sensitive to He bubbles [14]. As shown in Fig. 1b, the n/m ratio of He_nV_m clusters increases with depth, while the increasing number of He atoms in the He_nV_m clusters reduces the probability of positron annihilation by He_nV_m clusters [21] and subsequently leads to the further decline of the *S* value. Moreover, compared with the pristine film, the nanochannel structure in

the irradiated films are not detected by positron with increasing fluence, which may be due to the fact that positrons are annihilated in the He-vacancy clusters that accumulated at the surface of nanochannel.

According to the Arrhenius diffusion equation [9]:

$$D = D_0 \exp(-E_a / k_B T) \quad (4)$$

where D_0 is the pre-exponential factor, E_a is activation energy, k_B is Boltzmann constant, T is temperature. It is obviously expected that the irradiation temperature greatly affects the diffusion rate of defects and further affects the formation and evolution of vacancy-type defects. Some previous works have reported that when the annealing temperature is higher than 250 ºC, the monovacancies in the He-irradiated ordinary polycrystalline W start to mobile [19, 20, 37]. While as shown in Fig.3b, it is found that the types of vacancy-like defects in the W film irradiated at 300 ºC are almost unchanged compared with those irradiated at RT. This illustrates that although the monovacancies can mobile at 300 ºC, they do not promote the formation of larger He_nV_m clusters. It is possible that, at this temperature, the monovacancies start to migrate and bind with part of single He atoms or small He clusters, resulting in a slight increase in the number of the He_nV_m clusters and almost no change in the size of the He_nV_m clusters, which leads to a slight increase in *S* values. Since the diffusion and trapping rates of He atoms by vacancies or vacancy clusters both increase at 300°C, the He retention is nearly the same as that of the film irradiated at RT. When the temperature is further increased to 600 ºC, the diffusion rates of monovacancy and He atoms are significantly increased, even some small He clusters begin to migrate, resulting in the gradual formation of a number of larger He_nV_m clusters with low n/m ratio and even voids, which contributes to a substantial increase in *S* values of the film compared with those irradiated at RT and 300 ºC. Meanwhile, some

vacancy-like clusters can migrate and annihilate at defect sinks such as nanochannel surfaces, accompanied by the He release [19, 37]. Note that the existence of nanochannel structures greatly increases the density of defect sinks in the W film. And the distance of the He atoms or other vacancy-like clusters migrate to the nanochannel surface is shorter than those to flat surface of film. Thus, the nanochannel structures can enhance the release of He from the film.

Irradiation hardening is mainly induced by dislocation loops and He-vacancy clusters [40]. In this experiment, the effect of He-vacancy clusters on the irradiation hardening is mainly studied. Combined with the vacancy-type defects and He retention analysis, it can be concluded that the number and the size of He_nV_m clusters increase with increasing fluence, leading to the increase of hardness of the films. The significant increase in the hardness of the film irradiated to 5×10^{16} ions/cm^2 at RT may be due to the formation of small He bubbles. A slightly increase in the number of He_nV_m clusters continues to lead to an increase in hardness when the temperature is increased to 300 °C. Meanwhile, the larger He_nV_m clusters and voids form, which further increases the hardness of the film irradiated at 600 °C.

From the above analysis, it can be seen that the nanochannel structures can still efficiently facilitate the release of He from the film even at relatively low fluences, which effectively delay the formation of He bubbles in the initial stages.

5. Conclusion

In this study, the DBS and SIMS techniques were used to investigate the early stage evolution of the He-irradiation induced vacancy-type defects and He retention in the nanochannel W film and to further enrich our current understanding of the nanochannel W film with high radiation resistance applications. The existence of the

nanochannel structures increases the surface-to-volume ratio of film, thus introducing a higher density of defect sinks (nanochannel surfaces) in the film. The nanochannels greatly shorten the diffusion distance of He atoms and other defects, and effectively help the He escape from the film even at relatively low fluences. In addition, the results also show that irradiation fluence and temperature have great influence on the evolution of vacancy-type defects and He retention, as well as on the changes of mechanical properties such as hardness.

Acknowledgments

We thank the Natural Science Foundation of China (11475129, 11522543 and 11875207), the Natural Science Foundation of Hubei Province, China (2016CFA080), and the Fundamental Research Funds for the Central Universities for financial support. Wang thanks the support by the Center for Fundamental Understanding of Transport Under Reactor Extremes (FUTURE), a DOE energy frontier research center (EFRC) at Los Alamos National Laboratory and by the Center for Integrated Nanotechnologies (CINT), a DOE nanoscience user facility jointly operated by Los Alamos and Sandia National Laboratories.

References:

[1] J. Knaster, A. Moeslang, T. Muroga, Materials research for fusion, Nature Physics 12(5) (2016) 424-434.

[2] J. Marian, C.S. Becquart, C. Domain, S.L. Dudarev, M.R. Gilbert, R.J. Kurtz, D.R. Mason, K. Nordlund, A.E. Sand, L.L. Snead, T. Suzudo, B.D. Wirth, Recent advances in modeling and simulation of the exposure and response of tungsten to fusion energy conditions, Nuclear Fusion 57(9) (2017) 092008.

[3] M. Thompson, D. Drummond, J. Sullivan, R. Elliman, P. Kluth, N. Kirby, D. Riley, C.S. Corr, Effect of W self-implantation and He plasma exposure on early-stage defect and bubble formation in tungsten, Nuclear Fusion 58(6) (2018) 066010.

[4] L. Sandoval, D. Perez, B.P. Uberuaga, A.F. Voter, Competing Kinetics and He Bubble Morphology in W, Physical Review Letters 114(10) (2015) 105502.

[5] K.D. Hammond, I.V. Naeger, W. Widanagamaachchi, L.-T. Lo, D. Maroudas, B.D. Wirth, Helium flux effects on bubble growth and surface morphology in plasma-facing tungsten from large-scale molecular dynamics simulations, Nuclear Fusion 59(6) (2019) 066035.

[6] Z. Yang, S. Blondel, K.D. Hammond, B.D. Wirth, Kinetic Monte Carlo Simulations of Helium Cluster Nucleation in Tungsten with Preexisting Vacancies, Fusion Science and Technology 71(1) (2017) 60-74.

[7] M.J. Baldwin, R.P. Doerner, Formation of helium induced nanostructure ‘fuzz’ on various tungsten grades, Journal of Nuclear Materials 404(3) (2010) 165-173.

[8] W. Qin, F. Ren, R.P. Doerner, G. Wei, Y. Lv, S. Chang, M. Tang, H. Deng, C. Jiang, Y. Wang, Nanochannel structures in W enhance radiation tolerance, Acta Materialia 153 (2018) 147-155.

[9] W. Qin, Y. Wang, M. Tang, F. Ren, Q. Fu, G. Cai, L. Dong, L. Hu, G. Wei, C. Jiang, Microstructure and hardness evolution of nanochannel W films irradiated by helium at high temperature, Journal of Nuclear Materials 502 (2018) 132-140.

[10] W. Qin, F. Ren, J. Zhang, X. Dong, Y. Feng, H. Wang, J. Tang, G. Cai, Y. Wang, C. Jiang, Helium retention in krypton ion pre-irradiated nanochannel W film, Nuclear Fusion 58(2) (2018) 026021.

[11] R. Ramachandran, C. David, R. Rajaraman, B.K. Panigrahi, G. Amarendra, Evolution, migration and clustering of helium-vacancy complexes in RAFM steel-

depth resolved positron annihilation Doppler broadening study, Philosophical Magazine 96(22) (2016) 2385-2396.

[12] B. Xiong, W. Mao, X. Tang, C. He, Positron annihilation characteristics in mesostructural silica films with various porosities, Journal of Applied Physics 115(9) (2014) 094303.

[13] P. Peres, S.Y. Choi, F. Desse, P. Bienvenu, I. Roure, Y. Pipon, C. Gaillard, N. Moncoffre, L. Sarrasin, D. Mangin, Dynamic SIMS for materials analysis in nuclear science, Journal of Vacuum Science & Technology B, Nanotechnology and Microelectronics: Materials, Processing, Measurement, and Phenomena 36(3) (2018) 03F117.

[14] M. Cui, C. Yao, T. Shen, L. Pang, Y. Zhu, B. Li, X. Cao, P. Zhang, J. Sun, H. Zhu, J. Wang, X. Gao, N. Gao, H. Chang, Y. Sheng, H. Zhang, Z. Wang, Slow positron annihilation studies on helium irradiated tungsten, Nuclear Instruments and Methods in Physics Research Section B: Beam Interactions with Materials and Atoms 406 (2017) 578-584.

[15] M. Cui, Z. Wang, L. Pang, T. Shen, C. Yao, B. Li, J. Li, X. Cao, P. Zhang, J. Sun, Y. Zhu, Y. Li, Y. Sheng, Temperature dependent defects evolution and hardening of tungsten induced by 200keV He-ions, Nuclear Instruments and Methods in Physics Research Section B: Beam Interactions with Materials and Atoms 307 (2013) 507-511.

[16] A. Hasegawa, M. Fukuda, K. Yabuuchi, S. Nogami, Neutron irradiation effects on the microstructural development of tungsten and tungsten alloys, Journal of Nuclear Materials 471 (2016) 175-183.

[17] X. Ou, W. Anwand, R. Kögler, H. Zhou, A. Richter, The role of helium implantation induced vacancy defect on hardening of tungsten, Journal of Applied Physics 115(12) (2014) 123521.

[18] S. Jin, P. Zhang, E. Lu, L. Guo, B. Wang, X. Cao, Correlation between Cu precipitates and irradiation defects in Fe–Cu model alloys investigated by positron annihilation spectroscopy, Acta Materialia 103 (2016) 658-664.

[19] A. Debelle, M.F. Barthe, T. Sauvage, First temperature stage evolution of irradiation-induced defects in tungsten studied by positron annihilation spectroscopy, Journal of Nuclear Materials 376(2) (2008) 216-221.

[20] P.E. Lhuillier, T. Belhabib, P. Desgardin, B. Courtois, T. Sauvage, M.-F. Barthe, A.-L. Thomann, P. Brault, Y. Tessier, Trapping and release of helium in tungsten, Journal of Nuclear Materials 416(1) (2011) 13-17.

[21] X. Zhu, Y. Zhang, L. Cheng, Y. Yuan, G.D. Temmerman, B. Wang, X. Cao, G. Lu, Deuterium occupation of vacancy-type defects in argon-damaged tungsten exposed to high flux and low energy deuterium plasma, Nuclear Fusion 56(3) (2016) 036010.

[22] H. Lefaix-Jeuland, S. Moll, F. Legendre, F. Jomard, SIMS depth profiling of implanted helium in pure iron using CsHe+ detection mode, Nuclear Instruments and Methods in Physics Research Section B: Beam Interactions with Materials and Atoms 295 (2013) 69-71.

[23] Q. Cao, X. Ju, L. Guo, B. Wang, Helium-implanted CLAM steel and evolutionary behavior of defects investigated by positron-annihilation spectroscopy, Fusion Engineering and Design 89(7–8) (2014) 1101-1106.

[24] Y. Xin, X. Ju, J. Qiu, L. Guo, J. Chen, Z. Yang, P. Zhang, X. Cao, B. Wang, Vacancy-type defects and hardness of helium implanted CLAM steel studied by

positron-annihilation spectroscopy and nano-indentation technique, Fusion Engineering and Design 87(5–6) (2012) 432-436.

[25] H. Zhang, F. Ren, Y. Wang, M. Hong, X. Xiao, D. Liu, W. Qin, X. Zheng, Y. Liu, C. Jiang, Enhanced radiation tolerance of nanochannel V films through defects release, Nuclear Instruments and Methods in Physics Research Section B: Beam Interactions with Materials and Atoms 334 (2014) 1-7.

[26] H. Wang, F. Ren, J. Tang, W. Qin, L. Hu, L. Dong, B. Yang, G. Cai, C. Jiang, Enhanced radiation tolerance of YSZ/Al2O3 multilayered nanofilms with pre-existing nanovoids, Acta Materialia 144 (2018) 691-699.

[27] W.D. Nix, H. Gao, Indentation size effects in crystalline materials: A law for strain gradient plasticity, Journal of the Mechanics and Physics of Solids 46(3) (1998) 411-425.

[28] R. Kasada, Y. Takayama, K. Yabuuchi, A. Kimura, A new approach to evaluate irradiation hardening of ion-irradiated ferritic alloys by nano-indentation techniques, Fusion Engineering and Design 86(9-11) (2011) 2658-2661.

[29] Y. Takayama, R. Kasada, Y. Sakamoto, K. Yabuuchi, A. Kimura, M. Ando, D. Hamaguchi, H. Tanigawa, Nanoindentation hardness and its extrapolation to bulk-equivalent hardness of F82H steels after single- and dual-ion beam irradiation, Journal of Nuclear Materials 442(1, Supplement 1) (2013) S23-S27.

[30] M.H. Cui, T.L. Shen, H.P. Zhu, J. Wang, X.Z. Cao, P. Zhang, L.L. Pang, C.F. Yao, K.F. Wei, Y.B. Zhu, B.S. Li, J.R. Sun, N. Gao, X. Gao, H.P. Zhang, Y.B. Sheng, H.L. Chang, W.H. He, Z.G. Wang, Vacancy like defects and hardening of tungsten under irradiation with He ions at 800 °C, Fusion Engineering and Design 121 (2017) 313-318.

[31] P.M. Gordo, M.F. Ferreira Marques, M.T. Vieira, Positron Annihilation Study on Nanocrystalline Copper Thin Films Doped with Nitrogen, 65 (2017) 15-24.

[32] Z.Q. Chen, M. Maekawa, A. Kawasuso, S. Sakai, H. Naramoto, Annealing process of ion-implantation-induced defects in ZnO: Chemical effect of the ion species, Journal of Applied Physics 99(9) (2006) 093507.

[33] M.H.J. 't Hoen, M. Mayer, A.W. Kleyn, H. Schut, P.A. Zeijlmans van Emmichoven, Reduced deuterium retention in self-damaged tungsten exposed to high-flux plasmas at high surface temperatures, Nuclear Fusion 53(4) (2013) 043003.

[34] L. Hu, K.D. Hammond, B.D. Wirth, D. Maroudas, Molecular-dynamics analysis of mobile helium cluster reactions near surfaces of plasma-exposed tungsten, Journal of Applied Physics 118(16) (2015) 163301.

[35] K.D. Hammond, B.D. Wirth, Crystal orientation effects on helium ion depth distributions and adatom formation processes in plasma-facing tungsten, Journal of Applied Physics 116(14) (2014) 143301.

[36] P.E. Lhuillier, A. Debelle, T. Belhabib, A.L. Thomann, P. Desgardin, T. Sauvage, M.F. Barthe, P. Brault, Y. Tessier, Helium desorption in 3He implanted tungsten at low energy, Journal of Nuclear Materials 417(1–3) (2011) 504-507.

[37] A. De Backer, P. Lhuillier, C. Becquart, M. Barthe, Modelling of the implantation and the annealing stages of 800keV 3 He implanted tungsten: Formation of nanovoids in the near surface region, Journal of Nuclear Materials 429(1) (2012) 78-91.

[38] P.E. Lhuillier, T. Belhabib, P. Desgardin, B. Courtois, T. Sauvage, M.F. Barthe, A.L. Thomann, P. Brault, Y. Tessier, Helium retention and early stages of helium-vacancy complexes formation in low energy helium-implanted tungsten, Journal of Nuclear Materials 433(1–3) (2013) 305-313.

[39] A. Richter, W. Anwand, C.-L. Chen, R. Böttger, Evaluation of defect formation in helium irradiated Y2O3 doped W-Ti alloys by positron annihilation and nanoindentation, Journal of Nuclear Materials 494 (2017) 294-302.

[40] D.E.J. Armstrong, P.D. Edmondson, S.G. Roberts, Effects of sequential tungsten and helium ion implantation on nano-indentation hardness of tungsten, Applied Physics Letters 102(25) (2013) 251901.

Table:

Table 1. He retention fluence in the irradiated nanochannel W films obtained from the He quantified depth profiles. Two depth profiling measurements were performed for each sample.

Fluence (ions/cm^2)	Temp (°C)	He retention fluence (atom/cm^2)	Average He retention fluence (atom/cm^2)
5×10^{15}	RT	5.00×10^{15} 4.97×10^{15}	4.99×10^{15}
1×10^{16}	RT	0.77×10^{16} 0.78×10^{16}	0.78×10^{16}
5×10^{16}	RT	2.86×10^{16} 2.82×10^{16}	2.84×10^{16}
5×10^{16}	300	2.91×10^{16} 2.87×10^{16}	2.89×10^{16}
5×10^{16}	600	1.66×10^{16} 1.65×10^{16}	1.65×10^{16}

Figure Captions:

Fig. 1. (a) Cross-sectional TEM image of the nanochannel W film, (b) the depth profiles of He atoms and vacancies in the nanochannel W film (17.46 g/cm^3) irradiated by 190 keV He^+ ions according to the SRIM-2013 results.

Fig. 2. *S* parameter (a_1, b_1) and corresponding $\Delta S/S$ parameter (a_2, b_2) as a function of the positron energy (bottom) and corresponding mean depth (top) in the nanochannel W film irradiated by 190 keV He^+ ions. (a_1, a_2) The pristine film irradiated at RT to the fluences of 5×10^{15}, 1×10^{16} and 5×10^{16} ions/cm^2, (b_1, b_2) the film irradiated to 5×10^{16} ions/cm^2 at RT, 300 °C, 600 °C, respectively.

Fig. 3. *W-S* plots of the nanochannel W film irradiated by 190 keV He^+ ions. (a) The pristine film irradiated at RT to the fluences of 5×10^{15}, 1×10^{16} and 5×10^{16} ions/cm^2, (b) the film irradiated to 5×10^{16} ions/cm^2 at RT, 300 °C, 600 °C, respectively. The arrow point means an increase in depth.

Fig. 4. He quantified depth profiles obtained by SIMS in nanochannel W film samples irradiated with 190 keV He^+ ions at different fluences and temperatures.

Fig. 5. Depth (h) dependents average hardness (H) profiles (a) and the H^2-1/h plots (b) of the pristine nanochannel W film irradiated by 190 keV He^+ ions at different

temperatures to several fluences. (c) Hardness (H_0) of each film calculated from (b) and their corresponding hardness increment.

Figures:

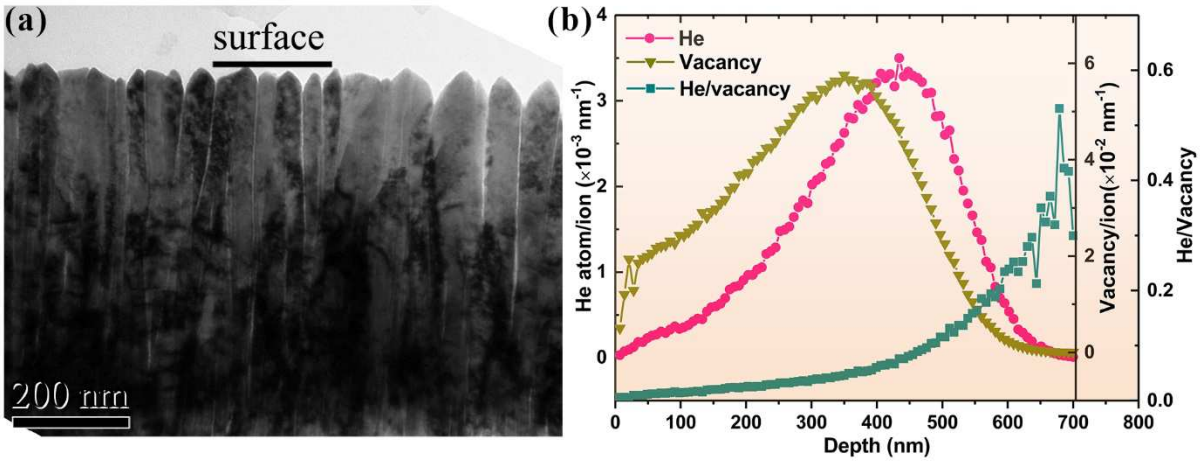

Fig.1

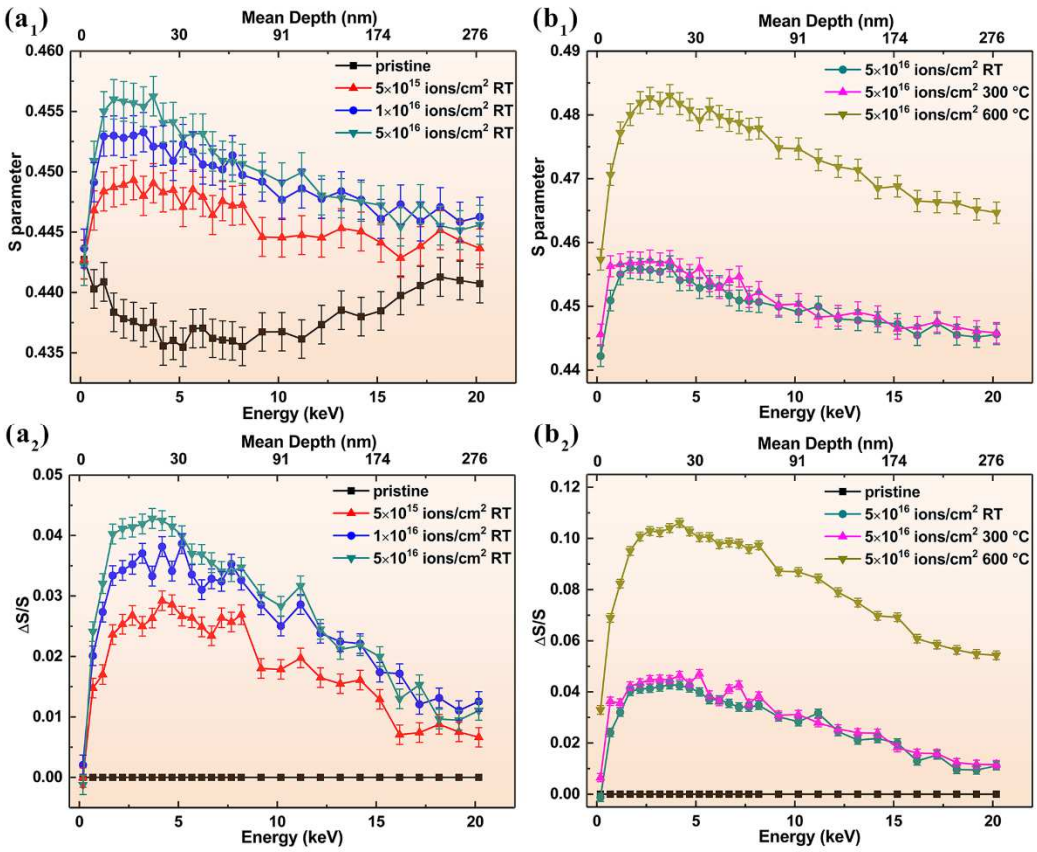
(a1)
Mean Depth (nm)
0
30
91
174
276
S parameter
Energy (keV)
pristine
5×10^15 ions/cm^2 RT
1×10^16 ions/cm^2 RT
5×10^16 ions/cm^2 RT
(b1)
5×10^16 ions/cm^2 RT
5×10^16 ions/cm^2 300 °C
5×10^16 ions/cm^2 600 °C
(a2)
ΔS/S
(b2)

Fig. 2

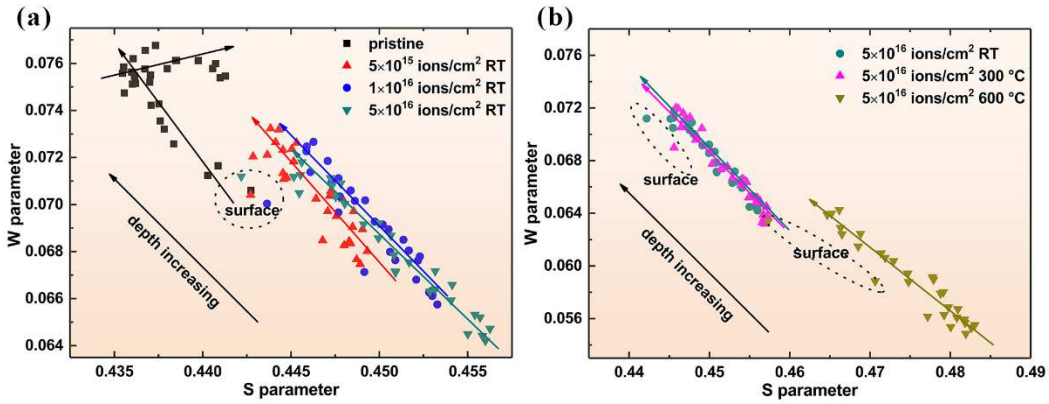
(a)
W parameter
S parameter
pristine
5×10^15 ions/cm^2 RT
1×10^16 ions/cm^2 RT
5×10^16 ions/cm^2 RT
surface
depth increasing
(b)
5×10^16 ions/cm^2 RT
5×10^16 ions/cm^2 300 °C
5×10^16 ions/cm^2 600 °C

Fig. 3

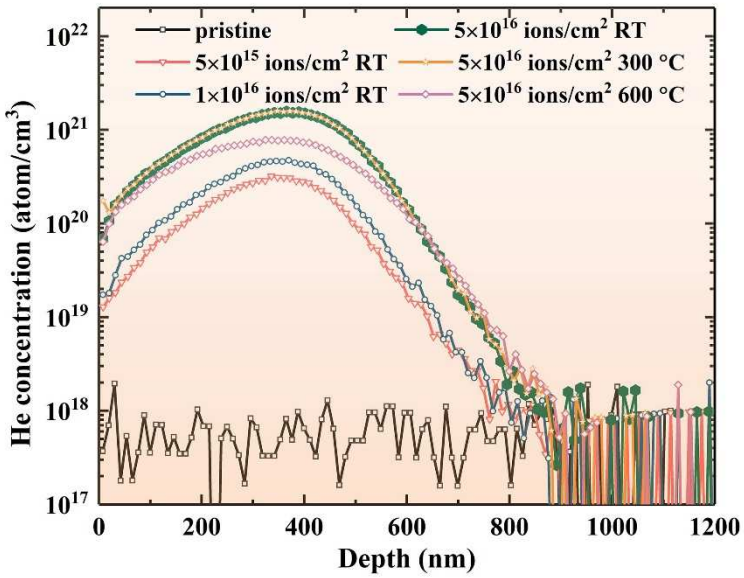

Fig. 4

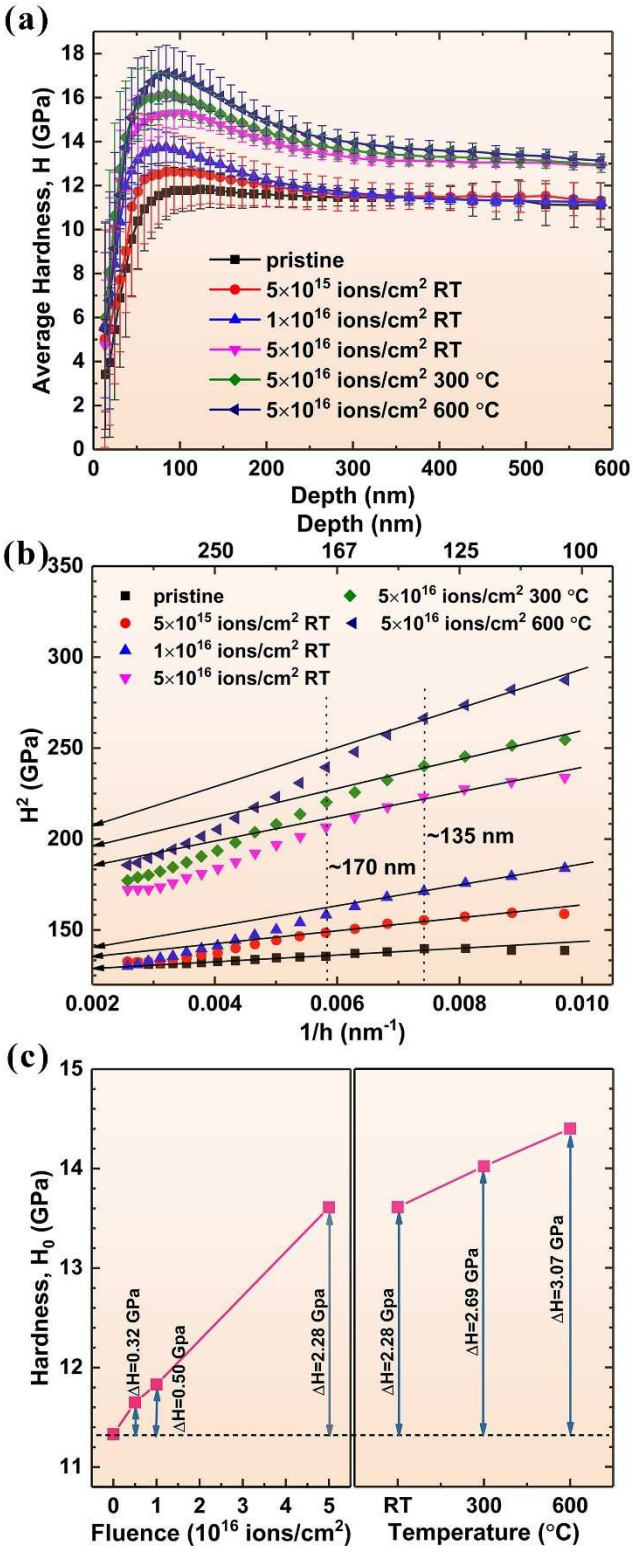
(a)
Average Hardness, H (GPa)
Depth (nm)
pristine
5×10^15 ions/cm^2 RT
1×10^16 ions/cm^2 RT
5×10^16 ions/cm^2 RT
5×10^16 ions/cm^2 300 °C
5×10^16 ions/cm^2 600 °C
(b)
Depth (nm)
H^2 (GPa)
1/h (nm^-1)
~135 nm
~170 nm
(c)
Hardness, H0 (GPa)
ΔH=0.32 GPa
ΔH=0.50 Gpa
ΔH=2.28 Gpa
ΔH=2.28 Gpa
ΔH=2.69 GPa
ΔH=3.07 GPa
Fluence (10^16 ions/cm^2)
Temperature (°C)

Fig. 5

Highlights:

1. The nanochannel structures facilitate He release from the film even at relatively low fluences.

2. Combined the advantage of DBS and SIMS methods to explore the evolution of helium-vacancy complex.

3. The irradiation fluence and temperature have great influence on the evolution of vacancy-type defects and He retention, as well as on the changes of hardness.

Conflict of Interest: The authors declare no conflict of interest.